https://doi.org/10.1007/s11467-023-1387-y

RESEARCH ARTICLE

Room-temperature ferromagnetism and half-metallicity in monolayer orthorhombic CrS_2

Bocheng Lei (雷博程)[1,3], Aolin Li (李奥林)[1*], Wenzhe Zhou (周文哲)[2], Yunpeng Wang (王云鹏)[2], Wei Xiong (熊威)[1], Yu Chen (陈羽)[2], Fangping Ouyang (欧阳方平)[1,2,4*]

[1]School of Physics Science and Technology, and Xinjiang Key Laboratory of Solid-State Physics and Devices, Xinjiang University, Urumqi 830046, China

[2]School of Physics, and Hunan Key Laboratory for Super-Microstructure and Ultrafast Process, and Hunan Key Laboratory of Nanophotonics and Devices, Central South University, Changsha 410083, China

[3]School of Physics Science and Technology, and Xinjiang Laboratory of Phase Transitions and Microstructures in Condensed Matter Physics, Yili Normal University, Yining, 835000, China;

[4]Powder Metallurgy Research Institute and State Key Laboratory of Powder Metallurgy, Central South University, Changsha 410083, China

Corresponding authors. E-mail: †liaolin628@xju.edu.cn, ‡ouyangfp06@tsinghua.org.cn

Received October 11, 2023; accepted January 9, 2024

Supplementary Information

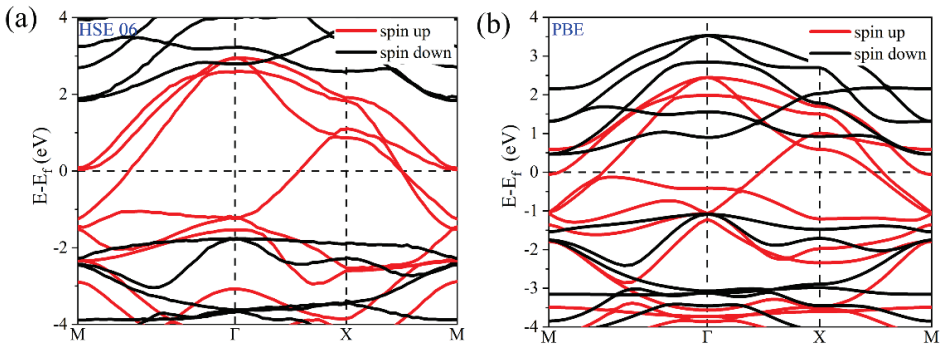

Fig. S1 Band structure calculated by HSE06 and PBE method (red line shows spin-up channel, black line shows spin-down channel). The Fermi level is denoted by a dashed line at 0.0 eV. The band structures do not appreciably change with respect to those obtained from HSE06 and PBE.

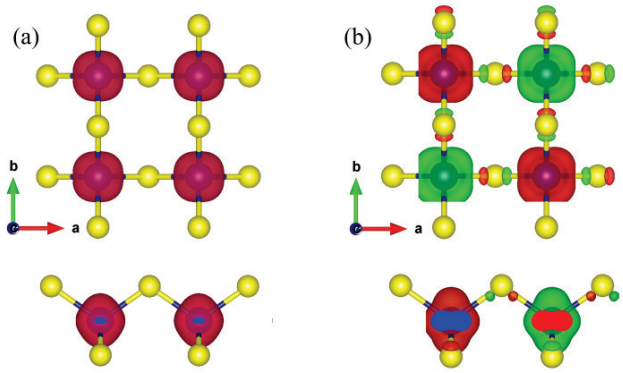

Fig. S2 (a) Ferromagnetic and **(b)** antiferromagnetic spin-charge density in unstrain.

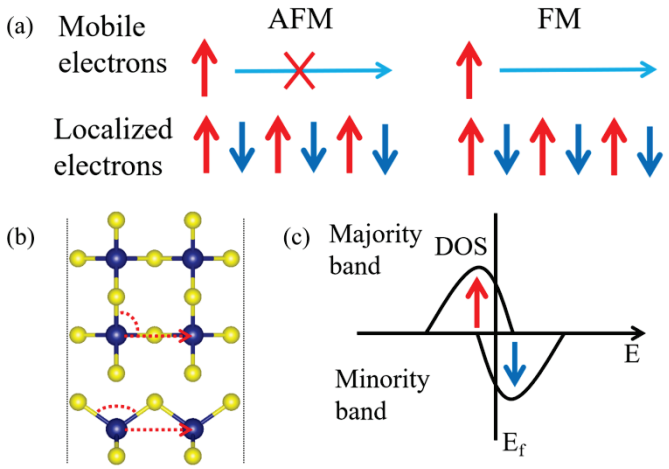

Fig. S3 The exchange mechanism of **(a)** double exchange, **(b)** direct exchange and super-exchange, and **(c)** itinerant ferromagnetism, respectively.

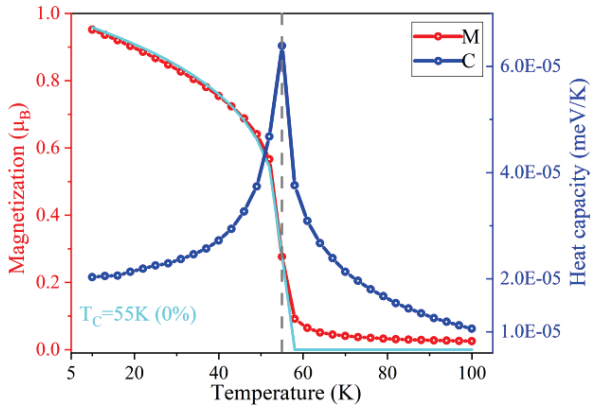

Fig. S4 The changing situation of total magnetization and specific heat of monolayer CrI_3 using Monte Carlo simulation, in which the fitting results are represented by cyan lines[1].

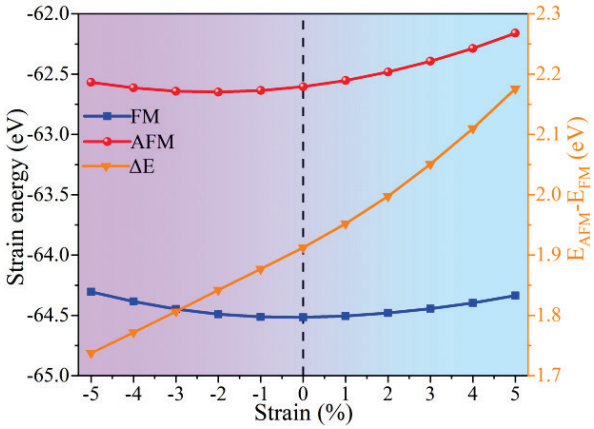

Fig. S5 The energy of FM and AFM configurations of ML O-CrO_2 under biaxial strain and the corresponding exchange energy.

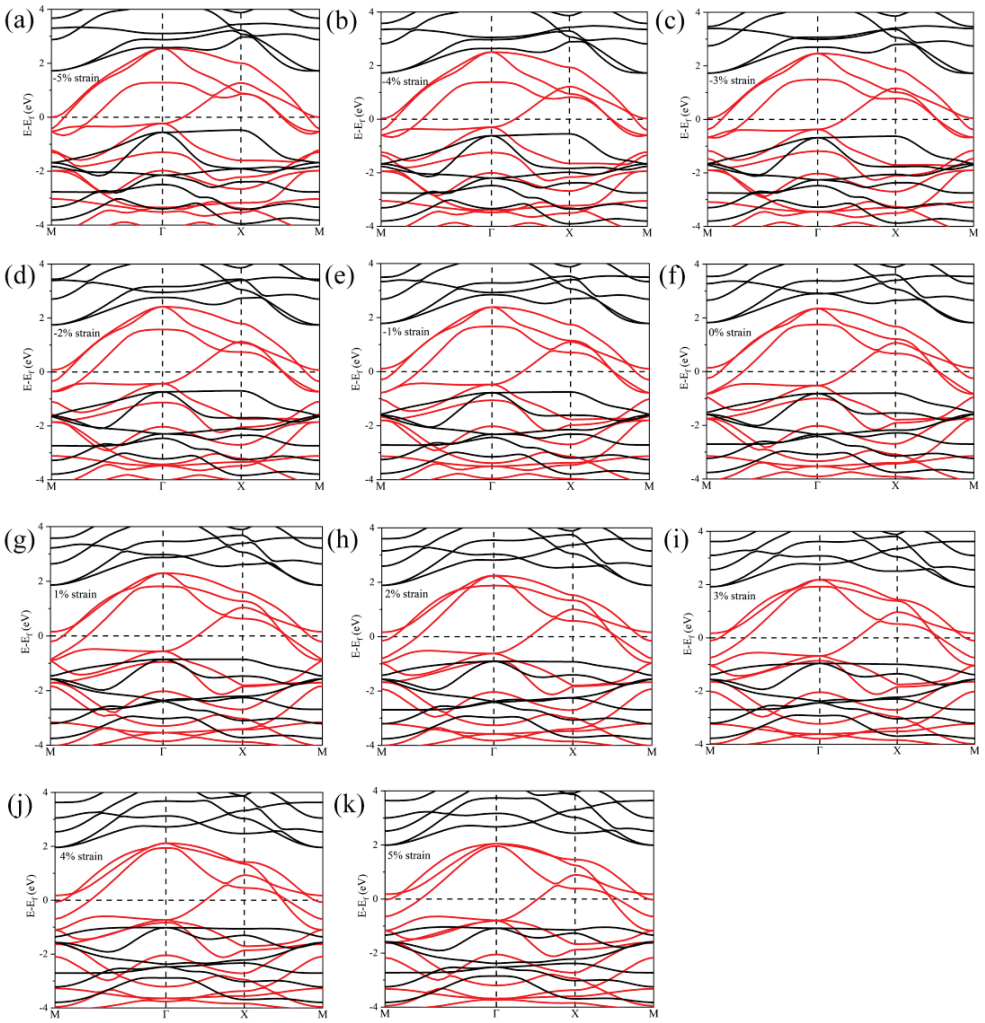

Fig. S6 Biaxial strain band structure, the red line indicates spin-up channel, the black line indicates spin-down channel. The Fermi level is denoted by a dashed line at 0.0 eV. The electronic band structures do not appreciably change with respect to those obtained from PBE+*U*.

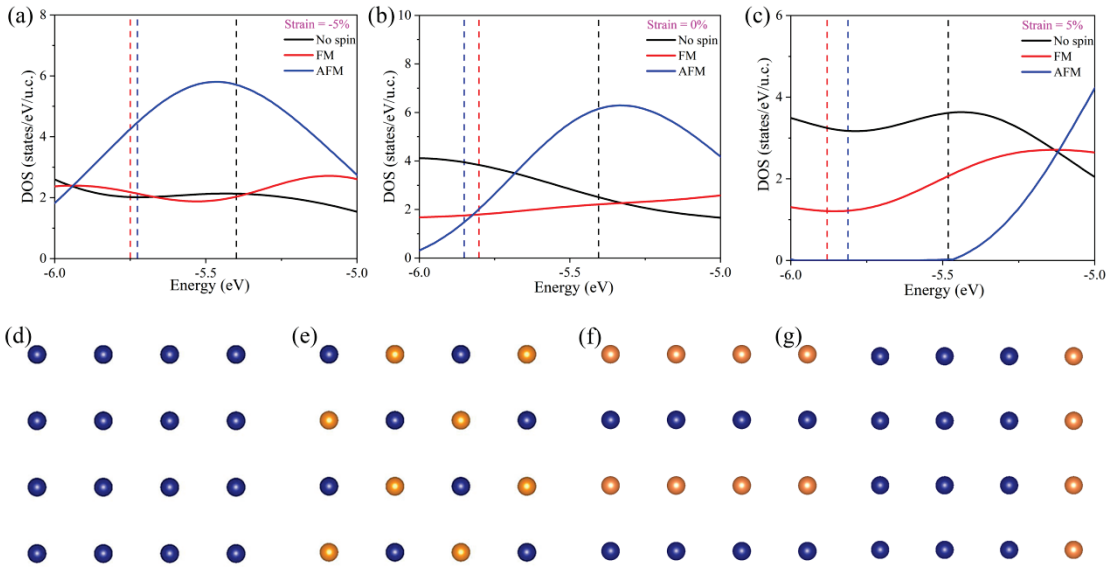

Fig. S7 The density of states for NM, FM, and AFM configurations at **(a)** –5% compressive strain, **(b)** 0% unstrain, and **(c)** 5% tensile strain. The magnetic configurations of ML O-CrS_2 within 4x4 supercell, as shown in **(d)–(g)**. The blue (orange) spheres represent the majority spin-up (-down) states.

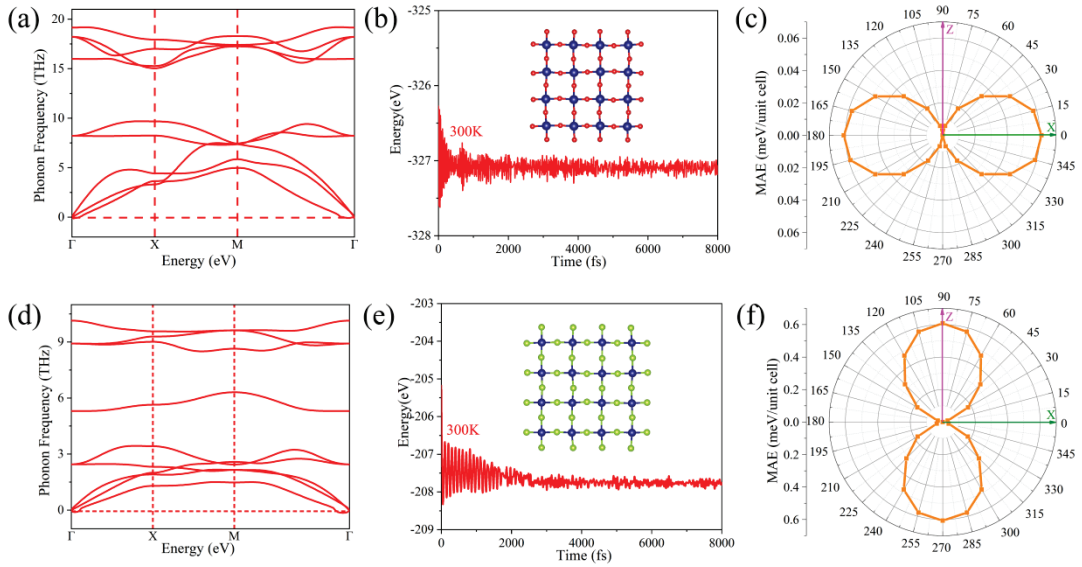

Fig. S8 (a,d) Phonon spectrum of the ML O-CrO_2 (O-$CrSe_2$) without obviously imaginary frequencies. **(b,e)** Variation of total potential energy E_0 during AIMD simulation at 300 K, and the inset shows the corresponding snapshots of structures at the end of 8 ps. **(c,f)** The energy variation of the magnetic anisotropy in the *XZ* plane.

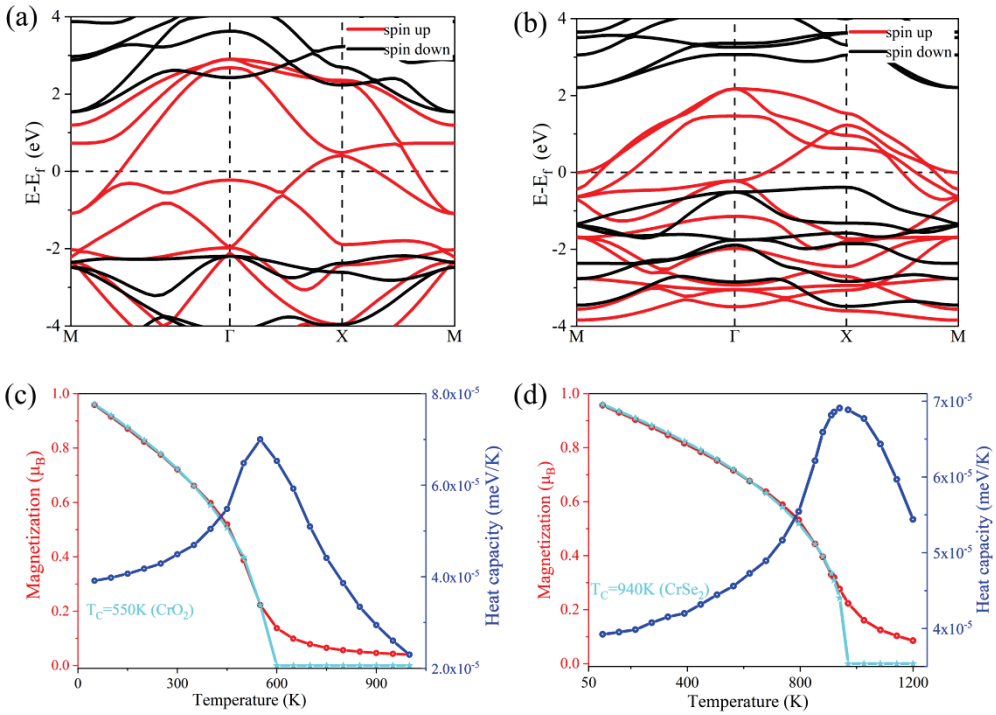

Fig. S9 (a,b) Band structure of the ML O-CrO_2 (O-$CrSe_2$) with red(black) lines indicating spin-up or spin-down channel. **(c,d)** The evolution of total magnetization and specific heat of ML O-CrO_2 (O-$CrSe_2$), obtained from MC simulation, with the fitting results are represented by cyan lines.

In our study, we also constructed CrX_2 (X = O/Se), a homolog of CrS_2. The ground state of both compounds is FM with a magnetic moment of approximately 2 μ_B. The FM energy of CrO_2/$CrSe_2$ is 1.174/2.074 eV/unit cell lower than that of the AFM case. The optimized lattice constants, magnetic anisotropies, and magnetic moments of CrX_2 (X = O/Se) are summarized in Table S5. According to Fig. S8 of the supplementary material, the calculated phonon

spectra and ab initio molecular dynamics(AIMD) indicate their thermodynamic stability. The calculated energy band structures and T_C of CrO_2 and $CrSe_2$ are plotted in Figure S9 of the Supplementary Materials. Both compounds are spin-up FM half-metallicity. It was further discovered that the T_C of both CrO_2 and $CrSe_2$ are very high, 550 K and 940 K, respectively. However, their lattice constants are significantly different (3.100/3.859), suggesting that the structural parameters do not particularly contribute to the FM exchange coupling. Instead, the T_C are primarily dominated by the exchange interaction of the itinerant electrons. When X changes from O to S to Se, the magnetic anisotropy energy of CrX_2 increases, which is related to the nonmetallic element X. The magnetization easy axis shifts from out-of-plane to in-plane. This study demonstrates that CrX_2 (X = O/Se) exhibits the same structure, FM order, and high T_C as CrS_2. Given these magnetic properties, it can serve as a critical component in various spintronic devices, including sources and sinks of spin-polarized current, spin-polarized electron memory, and spin field-effect transistors.

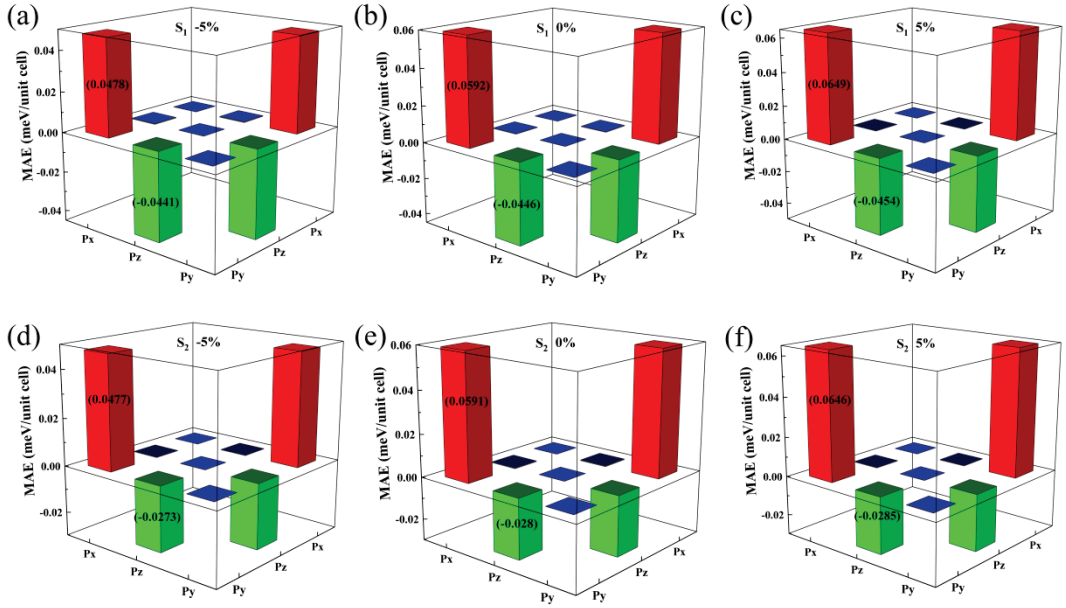

Fig. S10 The MAE mechanism analysis of ML O-CrS_2. orbital-resolved MAE of S_1(S_2) atoms at **(a,d)** -5% compressive strain, **(b,e)** 0% unstrain, and **(c,f)** 5% tensile strain.

Further, we analysed the IMA mechanism for the S-3p orbitals. Given that the mechanism of the IMA remains consistent for biaxial strains, we selected strains of –5%, 0%, and 5% as representative values. The orbital-resolved MAE, as depicted in Fig. S10, shows that for S atoms at strain values of –5%, the hybridizations of P_z with P_y (green bars) contributes to a PMA. Conversely, the hybridizations of P_x with P_y (red bars) results in a strong IMA contribution. The relatively smaller amplitude of the S anisotropy in ML O-CrS_2 can be attributed to the competition between these two hybridizations. As the strain increases (as shown in Figs. S10 (b–f)), both the PMA and IMA continue to rise, leading to a decrease in the overall MAE of the S atoms but an enhancement of the IMA. Therefore, for the ML O-CrS_2 system, the magnitude of the MAE is a consequence of the competition between Cr and S atoms.

Table S1 Magnetic correlation calculation parameters for different algorithms with FM as the ground state.

CrS_2	E(eV)	J (meV)	M_{Total} (μ_B)	M_{Cr} (μ_B)	M_{S1} (μ_B)	M_{S2} (μ_B)
FM(PBE)	0	63.188	1.930	2.231	-0.155	-0.146
AFM(PBE)	1.011		0	± 1.138	0	0
FM(PBE+U)	0	119.519	2.212	2.985	-0.373	-0.403
AFM(PBE+U)	1.920		0	± 2.415	0	0
FM(HSE06)	0	107.804	2.111	2.800	-0.356	-0.334
AFM(HSE06)	1.725		-0.314	2.016 -2.396	0.790	0.310

Table S2 Variation of the ground state energy, exchange energy ΔE, single-atom magnetic moment, and spin exchange parameters of monolayer orthorhombic CrS_2 with the value of U. The lattice constants and atomic positions are completely relaxed for each U, where $\Delta E=E_{AFM}–E_{FM}$.

CrS_2	E_{FM} (eV)	E_{AFM} (eV)	ΔE (eV)	J (meV)	M_{Cr} (μ_B)	M_{S1} (μ_B)	M_{S2} (μ_B)
U=0	0	0.999	0.999	62.496	2.238	–0.158	–0.149
U =1	0	1.410	1.410	88.118	2.471	–0.229	–0.223
U =2	0	1.701	1.701	106.324	2.714	–0.301	–0.299
U =3	0	1.912	1.912	119.519	2.985	–0.373	–0.403
U =4	0	2.059	2.059	128.709	3.197	–0.439	–0.450
U =5	0	2.094	2.094	130.848	3.410	–0.499	–0.518
U =2.8[2]	-	-	0.420	47.700	2.610	-	-
U =2.8[3]	0	-	0.318	-	2.206	-	-
U =3[4]	0	0.093	-	103.380	2.904	–0.244	–0.417

Table S3 Calculated parameters of magnetic correlation with biaxial strain.

ε (%)	M_{Total} (μ_B)	M_{Cr} (μ_B)	M_{S1} (μ_B)	M_{S2} (μ_B)	$E_{g\text{-}down}$ (eV)
–5	2.190	2.939	-0.348	–0.401	2.1949
–4	2.194	2.946	–0.352	–0.400	2.2746
–3	2.197	2.949	–0.355	–0.398	2.3552
–2	2.201	2.960	–0.360	–0.399	2.4436
–1	2.206	2.971	–0.365	–0.400	2.5358

0	2.212	2.985	–0.371	–0.403	2.6263
1	2.218	2.999	–0.377	–0.405	2.7145
2	2.223	3.010	–0.381	–0.406	2.7949
3	2.228	3.022	–0.386	–0.407	2.8795
4	2.235	3.038	–0.393	–0.410	2.9723
5	2.240	3.050	–0.398	–0.412	3.0264

Table S4 FM ground state energy, spin exchange parameters, and single-atom magnetic anisotropy energy at biaxial strain.

ε (%)	E_{FM} (eV)	ΔE (eV)	J (meV)	E_{MAE} (meV)
–5	0	1.738	108.600	–0.014
–4	0	1.772	110.725	–0.025
–3	0	1.806	112.897	–0.029
–2	0	1.842	115.119	–0.032
–1	0	1.877	117.311	–0.033
0	0	1.912	119.519	–0.034
1	0	1.952	121.995	–0.033
2	0	1.998	124.854	–0.025
3	0	2.051	128.170	–0.018
4	0	2.110	131.863	–0.016
5	0	2.176	135.993	–0.012

Table S5 Lattice constants a and b, MAE (meV) per Cr in different directions against the minimum energy spin orientation, single-atom magnetic moment M (μ_B) in the FM state.

	a=b (Å)	E_{100}	E_{010}	E_{001}	M_{total}	M_{Cr}	M_{S1}	M_{S2}
CrO_2	3.100	0	0	–0.058	1.982	2.389	–0.214	–0.193
$CrSe_2$	3.859	0	0	0.608	2.335	3.273	–0.448	–0.489

References

1. H. B. Wang, F. R. Fan, S. S. Zhu, and H. Wu, Doping enhanced ferromagnetism and induced half-metallicity in CrI_3 monolayer, *EPL* 114(4), 47001 (2016)

2. C. Wang, X. Y. Zhou, Y. H. Pan, J. S. Qiao, X. H. Kong, C.-C. Kaun, and W. Ji, Layer and doping tunable

ferromagnetic order in two-dimensional CrS_2 layers, *Phys. Rev. B* 97(24), 245409 (2018)

3. M. R. Habib, S. P. Wang, W. J. Wang, H. Xiao, S. M. Obaidulla, A. Gayen, Y. Khan, H. Z. Chen, and M. S. Xu, Electronic properties of polymorphic two-dimensional layered chromium disulphide, *Nanoscale* 11(42), 20123 (2019)

4. G. Xiao, W. Z. Xiao, Q. Chen, and L. L. Wang, Novel two-dimensional ferromagnetic materials CrX_2 (X = O, S, Se) with high Curie temperature, *J. Mater. Chem. C* 10(46), 17665 (2022)